LETTERS
https://doi.org/10.1038/s41567-019-0547-z
nature physics

Pairing states of composite fermions in double-layer graphene

J. I. A. Li[1,2,5], Q. Shi[2,5], Y. Zeng[2], K. Watanabe[3], T. Taniguchi[3], J. Hone[4] and C. R. Dean[2*]

Heterostructures of vertically stacked graphene double layers, separated by a thin tunnel barrier, provide a highly tunable system to explore strongly interacting electron states. This is because the interlayer Coulomb interactions can be sensitively tuned simply by varying the barrier thickness. Recent studies of double-layer graphene have shown that, in the quantum Hall effect regime, strong interlayer coupling can induce electron–hole pairing across the two layers, resulting in a superfluid phase of interlayer excitons[1–3]. Here, we report a series of emergent fractional quantum Hall effect (FQHE) states appearing under similar conditions. We find excellent agreement between the sequence of observable FQHE states and the theoretically proposed two-component composite-fermion (CF) model, where the CF quasiparticle construction results from both interlayer and intralayer interactions[4,5]. Most remarkably, we observe an additional series of incompressible states at fractional filling that do not fit within either the single- or two-component CF models. We interpret these states to result from residual pairing interactions between CFs, representing a new type of correlated ground state that is unique to graphene double-layer structures and not described by the conventional CF model.

Within the narrowly dispersing Landau levels (LLs) that define the quantum Hall effect regime, the kinetic energy is quenched. The resulting electron behaviour is therefore determined almost entirely by minimizing Coulomb repulsion. This results in a series of correlated states appearing at fractional LL filling, known as the fractional quantum Hall effect (FQHE)[6,7]. In double-layer quantum wells consisting of closely spaced parallel two-dimensional electron gases, even richer quantum Hall physics emerges. In the small-separation limit, the additional layer degree of freedom and interlayer Coulomb interactions lead to a variety of new correlated states that are tunable with interlayer separation and transverse displacement fields. Experimentally observed examples include formation of a superfluid exciton condensate[1–3,8–10] between electrons in one layer and holes in the other, occurring at total integer LL filling (half filling in each layer) and even-denominator FQHE states at 1/2 and 1/4 total filling[11–15]. Theoretical work has identified a host of other possible states at fractional total filling, some of which are expected to be exotic non-abelian states with topologically non-trivial excitations[4,16–21]. However, compared with single-layer systems the FQHE in double layers has been less explored experimentally, and many of these states remain unobserved.

Here we report measurement of the FQHE in dual-gated double-layer graphene heterostructures where the active regions consist of two graphene monolayers separated by a layer of hexagonal boron nitride (see Supplementary Information for details of the device structure). Several recent efforts have demonstrated that in double-layer graphene the hexagonal boron nitride spacer can be made as thin as 1–2 nm before interlayer tunnelling becomes relevant[2,3,22–25]. Consequently, the effective interlayer separation d/ℓ_B, which characterizes the interlayer coupling strength, can remain less than 0.5 for B field up to 30 T. This provides access to a previously unexplored regime in quantum Hall bilayers that combines strong intralayer (high B) and strong interlayer (small effective d) Coulomb repulsion, and in a device structure where the layer densities can be independently tuned. We identify insulating interlayer states with a Corbino geometry, which was previously shown to yield improved resolution of FQHE states in single layer-graphene devices[26], and confirm the nature of these states with Coulomb drag measurements in a Hall bar geometry.

In the single-component composite-fermion (CF) model, an even number of flux quanta are attached to each electron, transforming the strongly interacting electrons into a system of nearly independent CF quasiparticles (this transformation is illustrated in Fig. 1a). Owing to the flux attachment, each CF also moves in a reduced effective magnetic field, $B^\star = B - an\phi_0$, where n is the carrier density, $\phi_0 = h/e$ is the magnetic flux quantum and a is the number of flux quanta attached to each electron. At filling fraction $\nu = 1/a$ the effective magnetic field is precisely zero and the CFs behave as a metal with a well defined Fermi surface[27]. Away from these Fermi surfaces, the FQHE states at fractional electron filling are reinterpreted instead as effective integer quantum Hall states of CFs, where the effective CF filling fraction, $\nu^\star$, is related to the real electron filling, ν, by the relation $\nu^\star = \nu/(1 - a\nu)$. This remarkably simple construction makes it possible to interpret a wide range of complex behaviour associated with the correlated FQHE states within the context of a non-interacting single-particle picture[5].

Figure 1c shows bulk conductance versus filling fraction, measured in a monolayer graphene Corbino disk at $B = 36$ T. The data range spans a single branch of the lowest LL between $\nu = 0$ and $\nu = 1$. A large number of FQHE states are visible (fractional denominators as large as 15 are resolvable), confirming the excellent sample quality and transport resolution achievable in the Corbino geometry. The top axis in Fig. 1c labels the filling fraction of the CF LLs (referred to as Λ-levels) calculated from the above relation for the 2-flux ($a = 2$) and 4-flux ($a = 4$) series. The sequence of states and their hierarchy are in excellent agreement with the non-interacting single-component CF model[4,5].

For double-layer systems, an expanded two-component CF model has been proposed to account for both intra- and interlayer types of interaction[4,5]. In addition to the flux attachment scheme described above, an additional number of flux quanta penetrating one layer are attached to electrons of the opposite

[1]Department of Physics, Brown University, Providence, RI, USA. [2]Department of Physics, Columbia University, New York, NY, USA. [3]National Institute for Materials Science, Tsukuba, Japan. [4]Department of Mechanical Engineering, Columbia University, New York, NY, USA. [5]These authors contributed equally: J. I. A. Li, Q. Shi. *e-mail: cd2478@columbia.edu

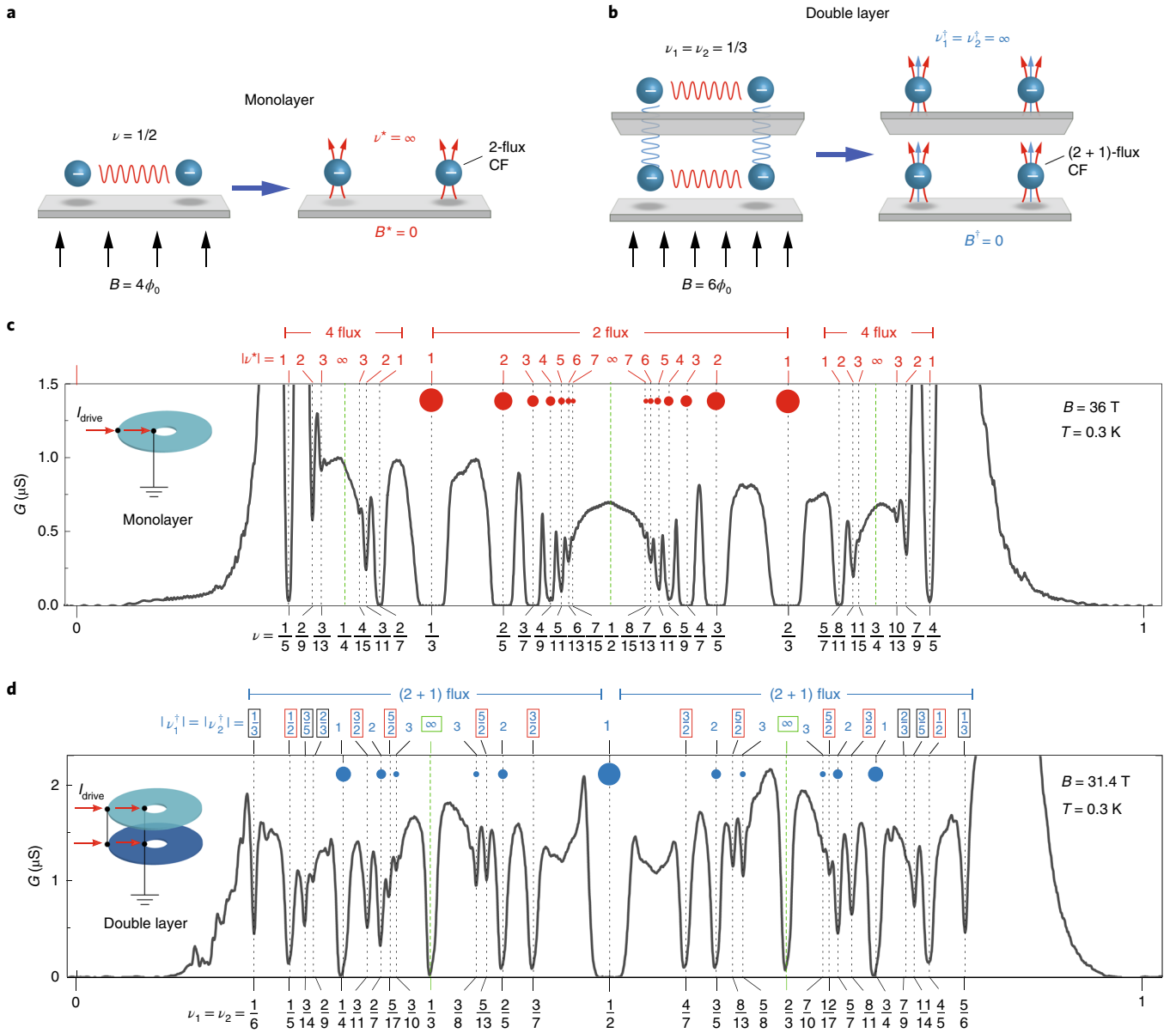

Fig. 1 | CF construction and bulk conductance measurement in Corbino geometry. a,**b**, Electron interactions within an LL can be modelled by attaching magnetic flux tubes to electrons to form non-interacting CFs. This process also modifies the effective magnetic field experienced by CFs, leading to an effective filling fraction that is different from that of the bare electrons. Zero effective field for CFs corresponds to LL filling $\nu = 1/2$ for single layers (**a**) and $\nu_1 = \nu_2 = 1/3$ for double layers (**b**) (see text). **c**, Bulk conductance, G, versus ν, measured in a single graphene Corbino disk. ν^* for the single-layer 2-flux and 4-flux CFs is indicated in red on the top axis. **d**, G versus $\nu_1 = \nu_2$ for a double-layer Corbino device, measured at equal layer densities. The corresponding effective filling, $\nu_i^\dagger$, for (2 + 1)-flux CFs is indicated in blue along the top axis (see text). Red and blue circles in **c** and **d**, respectively, highlight minima corresponding to integer-valued effective CF filling in each system. The circle radius is proportional to the width of the conductance minimum. Insets in **c** and **d** show the Corbino measurement geometry.

layer (we illustrate this as blue arrows in Fig. 1b). This construction renormalizes both the intra- and interlayer interactions, once again resulting in a system of nearly non-interacting CF quasiparticles. For this case the effective magnetic field seen by the CFs is determined by the electron density in both graphene layers, $B_i^\dagger = B - (an_i + bn_j)\phi_0$, where the subscripts i and j denote the layer index, and a and b are the numbers of intralayer and interlayer flux attachments, respectively. We note several important features of this transformation: (1) the CFs retain their layer index, but the layers become nearly independent of one another; (2) the CFs can experience different effective magnetic fields when the layer densities are not matched; (3) while the intralayer flux attachment must be an even number, the interlayer flux can be any integer value (but no larger than a). In this work we mainly consider two-component CF states with $a = 2$ and $b = 1$, which we refer to as a (2 + 1)-flux CF or ${}^2_1$CF for simplicity. While a and b can take on different integer values we find that the ${}^2_1$CF is dominant in the magnetic field and layer separation ranges that we discuss here (a detailed study of the interplay between different interlayer flux states will be presented elsewhere).

Figure 1d shows the electron transport response for a double-layer Corbino device with $d = 2.7$ nm interlayer spacing (this measurement is obtained in the matched-density condition with current

flowing through the two layers simultaneously, as depicted in the inset). We plot the bulk conductance versus individual layer filling fraction over the same range as in Fig. 1c, so that in the absence of interlayer interactions the two plots should be identical. However, it is clear on inspection that the presence of the second layer substantially modifies the response. While again we resolve a large number of FQHE states (labelled by the individual layer filling fraction on the bottom axis), the hierarchy of states shows no correlation to the single-layer response, and novel structures appear such as the condensate of electron–hole pairs at $\nu_1=\nu_2=\frac{1}{2}$ (that is, total electron filling fraction $\nu_{\mathrm{total}}=1$)[2,3].

In the two-component ${}^{2}_{1}$CF model, the effective Λ-level filling fraction at matched layer density is given by[4,5]

$$\nu_i^{\dagger}=\nu_j^{\dagger}=\frac{\nu}{1-3\nu} \tag{1}$$

where $\nu\equiv\nu_1=\nu_2$ and we use superscript † to distinguish this from the single-component CF model. For the hole-conjugate states at $1/2<\nu<1$, ν in equation (1) should be replaced by $1-\nu$. On the top axis of Fig. 1d we label the ${}^{2}_{1}$CF Λ-level filling fractions for each of the observed FQHE states. A prominent sequence of insulating features corresponding to integer values of $\nu_i^{\dagger}$ is evident, and its hierarchy is in excellent agreement with the two-component ${}^{2}_{1}$CF model, converging to the expected Fermi surface ($\nu_i^{\dagger}=\infty$) at electron LL filling $\nu_i=1/3$ and 2/3 (blue circles in Fig. 1d). However, a larger number of additional FQHE states are also present that do not correspond to integer filling of ${}^{2}_{1}$CF Λ-levels. These fall into three distinct categories: (1) fractional $\nu^{\dagger}$ with even denominator (highlighted by red squares in Fig. 1d), (2) fractional $\nu^{\dagger}$ with odd denominator (black squares) and (3) $\nu^{\dagger}=\infty$ ($\nu=1/3$ and 2/3), where a Fermi surface of CFs is expected (green squares). We note that incompressible states at a partially filled Λ-level, that is outside the integer CF Hall effect sequence, presumably involve correlation between CFs. An example of this kind of behaviour has been reported in GaAs single layers, where for example the $\nu=\frac{4}{11}$ state was argued to be a 1/3 FQHE of CFs, resulting from residual interactions between the CF quasiparticles[28]. In double layers, residual CF interactions play a more prominent role, stabilizing a wider variety of ground states with strength comparable to that of integer $\nu^{\dagger}$ (refs. [4,5]). The relative strength of fractional and integer $\nu^{\dagger}$ states indicates an effective Coulomb interaction different from a single two-dimensional confinement, due to the interlayer interaction.

Our dual-gated geometry allows us to independently tune the density of each layer and therefore map the evolution of these states away from the layer-balanced condition. Figure 2a plots bulk conductance as a function of $\nu_{\mathrm{total}}=\nu_1+\nu_2$ and the difference between the individual layer filling fractions, $\Delta\nu=\nu_1-\nu_2$. In the chosen colour scale dark blue indicates low conductance (either one or both layers is weakly conducting), while white indicates high conductance. Figure 2b summarizes the main features of Fig. 2a, where the solid lines identify prominent trajectories of low conductance. Open circles in Fig. 2b label the same layer-balanced ${}^{2}_{1}$CF states as were identified in Fig. 1d, where blue, red and black indicate integer, even-denominator and odd-denominator $\nu_i^{\dagger}$ states, respectively. Figure 2c plots a higher-resolution map of the dashed region in Fig. 2a, and Fig. 2d shows a corresponding contour plot where the sequence of incompressible states inside this dashed area can be seen in clearer detail.

For density imbalance between the layers, equation (1) can be generalized to

$$\nu_i^{\dagger}=\frac{\nu_i}{1-2\nu_i-\nu_j} \tag{2}$$

The dashed lines in Fig. 2b reflect lines of constant individual layer CF filling, according to equation (2). We observe that states appearing at integer $\nu_i^{\dagger}$ values under density balance evolve along trajectories (solid blue lines) that match the expected trajectories for integer filling of ${}^{2}_{1}$CF states in one layer (dashed blue lines). The intersection point between dashed blue lines, highlighted by blue circles in Fig. 2d, corresponds to regions where both layers are expected to have integer-valued $\nu_i^{\dagger}$ according to equation (2), and therefore both layers should be insulating. Figure 2c,d demonstrates robust insulating features at each of these crossing points, and shows a well defined hierarchy as judged by the depth of the conductance minimum: namely, the most robust ground states are observed at the four corners of the diamond-shaped area, where Λ-level filling is the lowest and the effective magnetic field is the strongest. The observed trajectories of the integer $\nu_i^{\dagger}$ states with layer imbalance, and their hierarchical behaviour, provide further evidence that these states are well described by the ${}^{2}_{1}$CF model.

Among the non-integer $\nu_i^{\dagger}$ states, the even-denominator states also evolve along lines of constant $\nu_i^{\dagger}$ (solid red lines in Fig. 2b) for half-filled ${}^{2}_{1}$CF Λ-levels (dashed red lines). As this trajectory is unique to the ${}^{2}_{1}$CF construction, it rules out the possibility of the ground state being an effective integer quantum Hall effect of other ${}^{a}_{b}$CFs. We note that along the red-line trajectories one of the layers remains at constant half-integer $\nu_i^{\dagger}$, while the other layer varies over a large range of effective filling. A state persisting along this trajectory therefore could indicate pairing between CFs within the half-Λ-filled layer only, with no correlation to the other layer. We speculate that these states may be of a similar origin to the Pfaffian that is believed to describe the half-filling even-denominator state in single-layer systems[4,29,30], though from the Corbino data alone we cannot definitively confirm this. At the matched-density condition, two copies of the presumed Pfaffian could persist, that is one in each layer, although interlayer correlations between the ${}^{2}_{1}$CFs could also play a role in determining the ground state here. In particular, we note the possibility of a CF exciton state[31] resulting from interlayer pairing of electron and hole ${}^{2}_{1}$CFs (ref. [31]) (Fig. 3a,b), in analogy to the condensate of electron–hole pairs that is observed when electrons occupy half-filled LLs in these same double layers[2,3]. We note that the even-denominator $\nu^{\dagger}$ states are stronger overall than the odd-denominator $\nu^{\dagger}$ states, a behaviour that is strikingly similar to the bare electron–hole bilayers, where the exciton condensate at half filling of each layer is generally the most dominant.

The odd-integer $\nu^{\dagger}=1/3$ states (black circles in Fig. 2b) disperse vertically with layer imbalance (solid black lines in Fig. 2b and highlighted by blue arrows in Fig. 2a,c,d) and show no correlation with behaviour expected for ${}^{2}_{1}$CF states. The state appearing at $\nu=\frac{1}{6}\left(\nu^{\dagger}=\frac{1}{3}\right)$, together with the observed insensitivity to layer imbalance, is consistent with the exciton condensate described by the Halperin Φ_{333} wavefunction, which has been theoretically predicted to stabilize in double-layer systems but not previously observed[16].

By contrast, the FQHE states at $\nu^{\dagger}=\infty$ ($\nu_i=1/3$ and 2/3) do not disperse at all with layer imbalance (green circles in Fig. 2b). We note that no state is expected here in the non-interacting ${}^{2}_{1}$CF picture since this filling corresponds to the expected Fermi surface. The pairing instability of such a Fermi surface, potentially giving rise to non-abelian incompressible states, has been the focus of theoretical discussion[4,18–20].

To distinguish among possible ground states we performed Coulomb drag measurements in a similar double-layer structure in which each layer is shaped into a Hall bar geometry (see Methods and Supplementary Information for detailed information on device geometry). In the Coulomb drag measurement, the Hall resistance of each layer exhibits a quantized plateau in the presence of an incompressible FQHE state, and the quantization value provides a topological invariant characteristic of the ground-state order[5,32]. For the integer ${}^{2}_{1}$CF filling states, marked by blue vertical lines in Fig. 3c, we observe zero-valued longitudinal drag resistance simultaneous with nearly quantized Hall resistance on both drag and drive layers

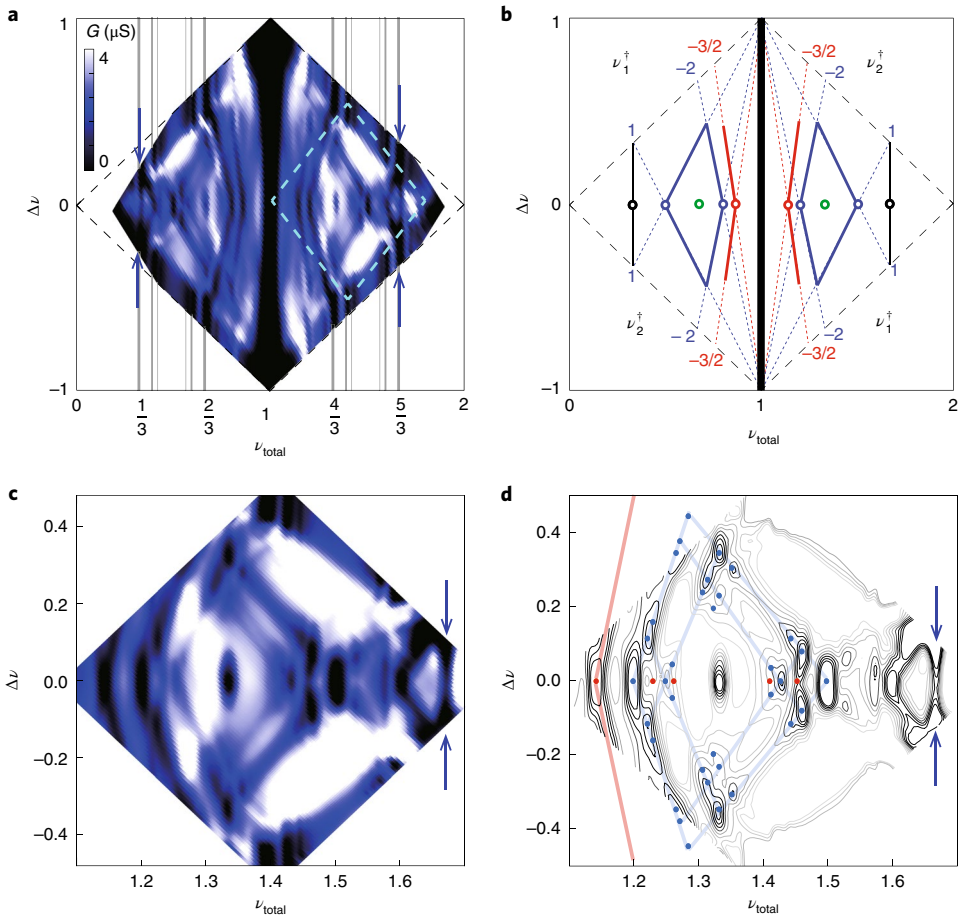

Fig. 2 | Density imbalance. a, G versus ν_{total} and $\Delta\nu$ measured at $B = 27$ T. **b**, Schematic phase diagram showing constant integer and half-integer CF filling in each graphene layer as dashed blue and red lines, respectively. Features observed in bulk conductance are highlighted as solid blue, red and black lines. The coloured circles correspond to insulating features in Fig. 1d under the matched-density condition. Blue, red and black circles mark integer, even-denominator and odd-denominator $\nu^{\dagger}$ states, respectively, whereas green circles correspond to $\nu_i = \frac{1}{3}$ and its particle–hole conjugate, where $^2_1$CFs form a Fermi surface phase. **c**, High-resolution measurement of the region highlighted by a dashed boundary in **a**, acquired at $B = 30$ T. **d**, Contour plot of bulk conductance data shown in **c**. Blue dots correspond to effective integer $^2_1$CF filling in both graphene layers. Red dots mark the effective half-filling states. Blue arrows point to the feature corresponding to the (333) state.

(Fig. 3c–e). In Fig. 3d,e we indicate the expected R_{xy}^{drag} and R_{xy}^{drive} plateau values according to the $^2_1$CF construction (Supplementary Information) by horizontal blue lines. We find good agreement with the measured values, providing further validation for the $^2_1$CF interpretation of these states[32].

For the even-denominator $^2_1$CF states (red vertical lines in Fig. 3c), the drag response demonstrates two types of behaviour depending on filling fraction range. At $\nu_i = \frac{3}{7}$, where $\nu^{\dagger} = 3/2$, the Hall resistance on both drive and drag layers approaches the expected plateau value for a composite exciton phase (red horizontal lines) with concomitant zero longitudinal drag resistance. Similar to the exciton condensate phase at $\nu_i = \frac{1}{2}$, such behaviour in Coulomb drag measurement is determined by the balance between counterflow current of composite excitons in sample bulk and quasiparticle current along the sample edge (see Supplementary Information for detailed calculation for composite exciton state)[2,3]. In the range $1/2 < \nu < 1$, the boundary condition combined with the edge mode configuration require the current flow through the device to be zero. Consequently both drive and drag layers are expected to exhibit insulating behaviour in the Coulomb drag geometry (Supplementary Information). Such insulating behaviour is clearly demonstrated by the resistance peak at $\nu_i = \frac{4}{7}$, which diverges with increasing B and exceeds 100 kΩ (Fig. 3c). Similar resistance peaks are present at $\nu_i = \frac{8}{13}$ and $\frac{8}{11}$. Taken together, Coulomb drag measurement in the matched-density condition provides strong evidence for exciton pairing between $^2_1$CFs (ref. [31]) when both graphene layers correspond to half-filled Λ-levels.

Finally, we briefly address the Coulomb drag response for the other two types of non-integer $^2_1$CF state. In Fig. 3c–e we observe a robust Hall resistance plateau at $\nu_i = \frac{2}{3}$, where a $^2_1$CF Fermi surface is expected. The drive- and drag-layer Hall resistances quantize to h/e^2 and $\frac{1}{2}h/e^2$, respectively, simultaneously with zero longitudinal resistance. This rules out the possibility of this feature being a conventional Laughlin state of two decoupled graphene layers[13,14], while providing direct evidence for a ground state with interlayer correlation. A detailed study of this behaviour with varying interlayer separation and magnetic field may resolve the origin of this state. However, we note that at present there is no theory of Hall drag associated with the pairing states that have been proposed for this filling fraction[4,18–20]. The odd-denominator $^2_1$CFs were not observable in our drag measurements (Fig. 3c–e), making it difficult to comment further beyond their observation in the Corbino measurement. We emphasize that the overall transport measurement resolution in the Hall bar geometry (Fig. 3) shows less resolution than our Corbino geometry (Fig. 1d), which is consistent with recent findings in monolayer graphene devices[26]. Further

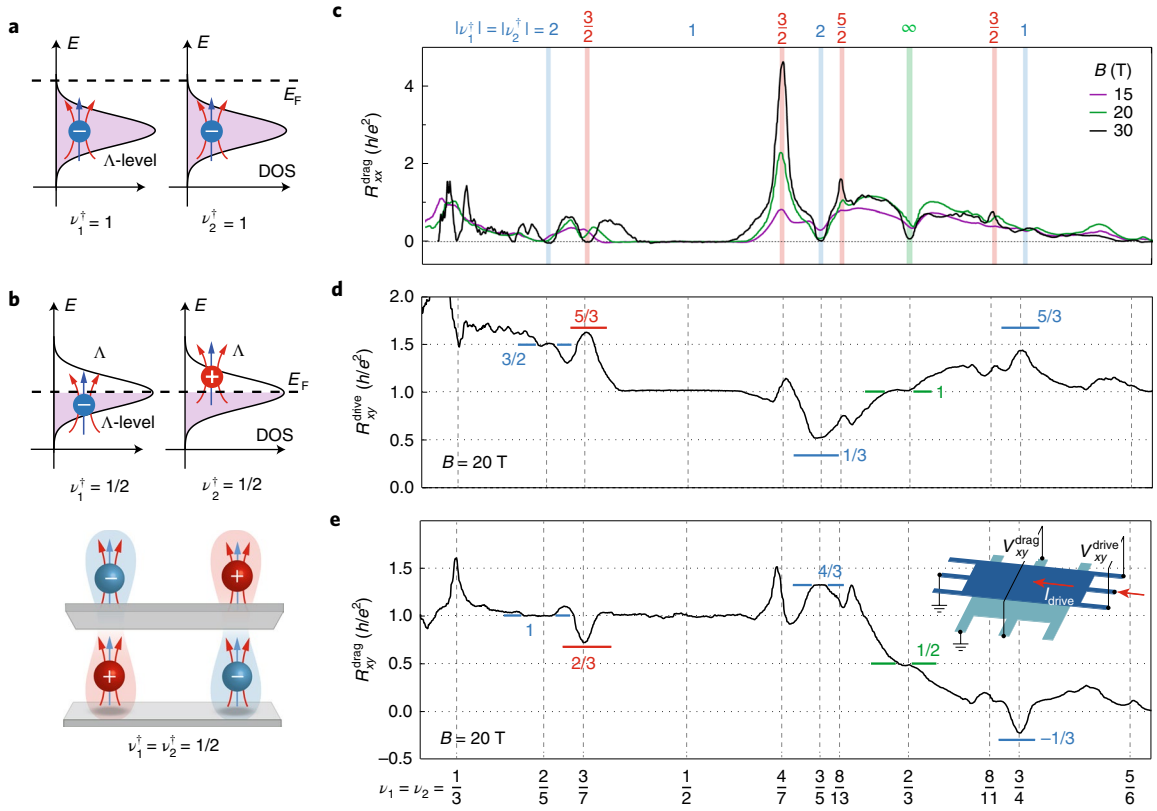

Fig. 3 | Coulomb drag measurement in Hall bar geometry. a,**b**, Schematic Λ-levels for different effective CF fillings. **a**, Integer CF filling for $^2_1$CF in both layers. **b**, Half-integer CF filling for $^2_1$CF in both layers. DOS, density of states. **c**–**e**, R_{xy}^{drive}, R_{xy}^{drag} and R_{xx}^{drag} versus ν_i along the equal-density line measured at $B = 20$ T and $T = 0.3$ K. Coulomb drag is performed on a device with $d = 2.5$ nm. Inset of **e**: schematic of Coulomb drag geometry (see Methods for more discussion).

investigation in improved Hall bar geometries will probably be required to resolve the nature of these states.

Overall, our observations suggest that the two-component CF construction for bilayers exhibits a self-similar correspondence to the bare electron bilayer behaviour but with residual interactions playing an important role. We note that interlayer coupling between the CFs remains evidently strong, and tunable, with effective layer separation providing a dynamic new way to study pairing between CFs. More generally, we establish double-layer graphene as a highly tunable system for studying pairing interaction between quasiparticles, and pave the way for systematic examination of exotic phases with novel topological and statistical properties.

Online content

Any methods, additional references, Nature Research reporting summaries, source data, statements of code and data availability and associated accession codes are available at https://doi.org/10.1038/s41567-019-0547-z.

Received: 11 January 2019; Accepted: 2 May 2019;
Published online: 24 June 2019

References

1. Eisenstein, J. P. Exciton condensation in bilayer quantum Hall systems. *Annu. Rev. Condens. Matter Phys.* **5**, 159–181 (2014).
2. Li, J. I. A., Taniguchi, T., Watanabe, K., Hone, J. & Dean, C. R. Excitonic superfluid phase in double bilayer graphene. *Nat. Phys.* **13**, 751–755 (2017).
3. Liu, X., Taniguchi, T., Watanabe, K., Halperin, B. & Kim, P. Quantum Hall drag of exciton condensate in graphene. *Nat. Phys.* **13**, 746–750 (2017).
4. Scarola, V. W. & Jain, J. K. Phase diagram of bilayer composite fermion states. *Phys. Rev. B* **64**, 085313 (2001).
5. Jain, J. K. *Composite Fermions* (Cambridge University Press, 2003).
6. Tsui, D. C., Stormer, H. L. & Gossard, A. C. Two-dimensional magnetotransport in the extreme quantum limit. *Phys. Rev. Lett.* **48**, 1559–1562 (1982).
7. Laughlin, R. B. Anomalous quantum Hall effect: an incompressible quantum fluid with fractionally charged excitations. *Phys. Rev. Lett.* **50**, 1395–1398 (1983).
8. Kellogg, M., Eisenstein, J. P., Pfeiffer, L. N. & West, K. W. Vanishing Hall resistance at high magnetic field in a double-layer two-dimensional electron system. *Phys. Rev. Lett.* **93**, 036801 (2004).
9. Tutuc, E., Shayegan, M. & Huse, D. A. Counterflow measurements in strongly correlated GaAs hole bilayers: evidence for electron–hole pairing. *Phys. Rev. Lett.* **93**, 036802 (2004).
10. Nandi, D., Finck, A. D. K., Eisenstein, J. P., Pfeiffer, L. N. & West, K. W. Exciton condensation and perfect Coulomb drag. *Nature* **488**, 481–484 (2012).
11. Halperin, B. I. Theory of the quantized Hall conductance. *Helv. Phys. Acta* **56**, 75–102 (1983).
12. Suen, Y. W., Engel, L. W., Santos, M. B., Shayegan, M. & Tsui, D. C. Observation of a $\nu = 1/2$ fractional quantum Hall state in a double-layer electron system. *Phys. Rev. Lett.* **68**, 1379–1382 (1992).
13. Eisenstein, J. P., Boebinger, G. S., Pfeiffer, L. N., West, K. W. & He, S. New fractional quantum Hall state in double-layer two-dimensional electron systems. *Phys. Rev. Lett.* **68**, 1383–1386 (1992).
14. Suen, Y., Manoharan, H., Ying, X., Santos, M. & Shayegan, M. Origin of the $\nu = 1/2$ fractional quantum Hall state in wide single quantum wells. *Phys. Rev. Lett.* **72**, 3405 (1994).
15. Shabani, J. et al. Phase diagrams for the stability of the $\nu = \frac{1}{2}$ fractional quantum Hall effect in electron systems confined to symmetric, wide GaAs quantum wells. *Phys. Rev. B* **88**, 245413 (2013).
16. Wen, X.-G. & Zee, A. Neutral superfluid modes and 'magnetic' monopoles in multilayered quantum Hall systems. *Phys. Rev. Lett.* **69**, 1811–1814 (1992).
17. Alicea, J., Motrunich, O. I., Refael, G. & Fisher, M. P. A. Interlayer coherent composite Fermi liquid phase in quantum Hall bilayers. *Phys. Rev. Lett.* **103**, 256403 (2009).
18. Ardonne, E., Lankvelt, F. J. Mv, Ludwig, A. W. W. & Schoutens, K. Separation of spin and charge in paired spin-singlet quantum Hall states. *Phys. Rev. B* **65**, 041305 (2002).

19. Barkeshli, M. & Wen, X.-G. Non-Abelian two-component fractional quantum Hall states. *Phys. Rev. B* **82**, 233301 (2010).
20. Geraedts, S., Zaletel, M. P., Papić, Z. & Mong, R. S. K. Competing Abelian and non-Abelian topological orders in $\nu=1/3+1/3$ quantum Hall bilayers. *Phys. Rev. B* **91**, 205139 (2015).
21. Liu, Z., Vaezi, A., Lee, K. & Kim, E.-A. Non-Abelian phases in two-component $\nu=2/3$ fractional quantum Hall states: emergence of Fibonacci anyons. *Phys. Rev. B* **92**, 081102 (2015).
22. Britnell, L. et al. Electron tunneling through ultrathin boron nitride crystalline barriers. *Nano Lett.* **12**, 1707–1710 (2012).
23. Gorbachev, R. V. et al. Strong Coulomb drag and broken symmetry in double-layer graphene. *Nat. Phys.* **9**, 775–779 (2013).
24. Li, J. I. A. et al. Negative Coulomb drag in double bilayer graphene. *Phys. Rev. Lett.* **117**, 046802 (2016).
25. Lee, K. et al. Giant frictional drag in double bilayer graphene heterostructures. *Phys. Rev. Lett.* **117**, 046803 (2016).
26. Zeng, Y. et al. High-quality magnetotransport in graphene using the edge-free Corbino geometry. *Phys. Rev. Lett.* **122**, 137701 (2019).
27. Halperin, B. I., Lee, P. A. & Read, N. Theory of the half-filled Landau level. *Phys. Rev. B* **47**, 7312–7343 (1993).
28. Pan, W. et al. Fractional quantum Hall effect of composite fermions. *Phys. Rev. Lett.* **90**, 016801 (2003).
29. Mukherjee, S., Mandal, S. S., Wójs, A. & Jain, J. K. Possible anti-Pfaffian pairing of composite fermions at $\nu=3/8$. *Phys. Rev. Lett.* **109**, 256801 (2012).
30. Mukherjee, S., Jain, J. K. & Mandal, S. S. Possible realization of a chiral p-wave paired state in a two-component system. *Phys. Rev. B* **90**, 121305 (2014).
31. Kamilla, R. K., Wu, X. G. & Jain, J. K. Excitons of composite fermions. *Phys. Rev. B* **54**, 4873–4884 (1996).
32. Renn, S. R. Edge excitations and the fractional quantum Hall effect in double quantum wells. *Phys. Rev. Lett.* **68**, 658–661 (1992).

Acknowledgements

This work was supported by the National Science Foundation (DMR-1507788) and by the David and Lucille Packard Foundation. Data analysis was partially supported by the US Department of Energy (DE-SC0016703). A portion of this work was performed at the National High Magnetic Field Laboratory, which is supported by National Science Foundation Cooperative Agreement No. DMR-1157490 and the State of Florida.

Author contributions

J.I.A.L. and C.R.D. designed the experiment. Experimental work and analysis was carried out by J.I.A.L., Q.S. and Y.Z., advised by J.H. and C.R.D. All authors contributed to writing the manuscript.

Competing interests

The authors declare no competing interests.

Additional information

Supplementary information is available for this paper at https://doi.org/10.1038/s41567-019-0547-z.

Reprints and permissions information is available at www.nature.com/reprints.

Correspondence and requests for materials should be addressed to C.R.D.

Peer review information: *Nature Physics* thanks G. J. Sreejith, Emanuel Tutuc and the other, anonymous, reviewer(s) for their contribution to the peer review of this work.

Publisher's note: Springer Nature remains neutral with regard to jurisdictional claims in published maps and institutional affiliations.

Methods

Charge-carrier density in top and bottom layers, n_{top} and n_{bot}, can be independently controlled by applying a voltage bias to the top and bottom graphite gate electrodes. Note that all measurements are performed with a hole-type charge carrier, with ν_1 and ν_2 denoting the LL filling of holes. Bulk conductance in parallel flow geometry is measured between the inner and outer edges of the Corbino shaped sample while changing the applied gate voltage on the top and bottom graphite electrodes. The interlayer separation is 3 nm for the device with Corbino geometry, and 2.5 nm in the device with Hall bar geometry.

In a sample with aligned Hall bar geometry as shown in the inset of Fig. 3c, Coulomb drag measurement is performed by flowing current in one graphene layer (the drive layer) while the other layer (the drag layer) is grounded. Longitudinal and Hall voltages are measured simultaneously on both graphene layers, which is made possible by shaping the double-layer structure into an aligned Hall bar geometry and making electrical contact to each graphene layer independently. The Hall resistance on the drive layer is defined as $R_{xy}^{drive} = V_{xy}^{drive}/I_{drive}$, whereas the longitudinal and Hall resistances on the drag layer are defined as $R_{xx}^{drag} = V_{xx}^{drag}/I_{drive}$ and $R_{xy}^{drag} = V_{xy}^{drag}/I_{drive}$, respectively. V_{xy}^{drive}, V_{xx}^{drag} and V_{xy}^{drag} are labelled in the inset of Fig. 3e. In the presence of a ground state with interlayer correlation, the Hall resistances in both drive and drag layers are expected to form a well-defined plateau, with the plateau value directly related to the nature of the interlayer correlation. At the same time zero longitudinal resistance is expected.

Data availability

The data that support the plots within this paper and other findings of this study are available from the corresponding author on reasonable request.